BOLETIN DE LA SOCIEDAD ESPAÑOLA DE
Cerámica y Vidrio
www.elsevier.es/bsecv

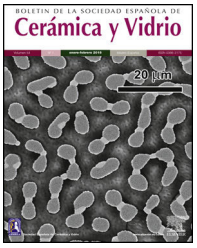

Synthesis of high crystallinity biphasic calcium phosphates/gold nanoparticles composites by solution combustion method with antimicrobial response

Alex Lopera[a,b], *Edgar Andrés Chavarriaga*[c], *Vinicius D.N. Bezzon*[d], *Mateo Zutta*[e,f], *Adrián Gómez*[b], *Jorge Puerta*[f], *Sara Maria Robledo*[g], *Victoria E. Ospina*[g], *Carlos Paucar*[a], *Claudia Garcia*[a,*]

[a] *Grupo de Cerámicos y Vítreos, Escuela de Física Universidad Nacional de Colombia, Calle 59A.63-20, Medellín 050034, Colombia*
[b] *Grupo GICEI-GIIEN, Institución Universitaria Pascual Bravo, Calle 73 No. 73A – 226, Medellín 050034, Colombia*
[c] *Departamento de Ciencias Básicas, Universidad Católica Luis Amigó, Transversal 51A # 67B 90, Medellín, Colombia*
[d] *Center for Natural and Human Sciences (CCNH), Federal University of ABC (UFABC), Santo André, SP, CEP 09210580, Brazil*
[e] *Departamento de Física, Facultad de Ciencias, Pontificia Universidad Javeriana, Carrera 7a No. 43-82, Bogotá, Colombia*
[f] *Grupo de Física Radiológica, Escuela de Física Universidad Nacional de Colombia, Calle 59A.63-20, Medellín 050034, Colombia*
[g] *PECET-Instituto de Investigaciones Médicas, Facultad de Medicina, Universidad de Antioquia, Calle 70 No. 52-21, Medellín 050010, Colombia*

ARTICLE INFO

Article history:
Received 20 September 2020
Accepted 26 March 2021
Available online 12 April 2021

Keywords:
Biphasic calcium phosphates
Gold nanoparticles
Solution combustion synthesis
High crystallinity
Antimicrobial

ABSTRACT

Calcium phosphates are biomaterials widely used in bone tissue engineering. In recent years, the alternative of obtaining these materials with antimicrobial properties, has been explored due to the multiple advantages that this would imply in the design of devices or implants that prevent the failure of these associated with bacterial colonization. The goal of the present work was obtaining gold nanoparticles supported on biphasic calcium phosphates (BCPs) with high crystallinity by one-step solution combustion technique, and with antimicrobial response, a fact that can significantly reduce the production cost of these materials. X-ray diffractograms (XRD) showed that prepared powders have high crystallinity owing to high temperatures during the combustion reaction, also Rietveld refinement showed that the inclusion of gold nanoparticles (AuNPs) influenced the phases' ratio obtained. Furthermore, scanning electron microscopy (SEM) showed agglomeration of particles with morphologies with shape tending to be equigranular, while the presence of AuNPs was corroborated by transmission electron microscopy (TEM). All samples that were obtained in a single step, by solution combustion, showed antimicrobial behavior validated through the inhibition halos, whereas particles subjected to thermal treatment lost their antimicrobial response.

* *Corresponding author.*
E-mail address: cpgarcia@unal.edu.co (C. Garcia).
https://doi.org/10.1016/j.bsecv.2021.03.007

Síntesis de materiales compuestos de fosfatos de calcio bifásicos/nanopartículas de oro de elevada cristalinidad, mediante el método de combustión de soluciones, con respuesta antimicrobiana

Palabras clave:
Fosfatos de calcio bifásicos
Nanopartículas de oro
Combustión de soluciones
Alta cristalinidad
Respuesta antimicrobiana

RESUMEN

Los fosfatos de calcio son biomateriales ampliamente usados en ingeniería de tejido óseo. En los últimos años, la alternativa de obtener estos materiales con propiedades antimicrobianas ha sido explorada debido a las múltiples ventajas que presentan en el diseño de dispositivos o implantes que incluyan la prevención de fallas asociadas a la colonización bacteriana. El principal objetivo de esta investigación fue obtener nanopartículas de oro soportadas en fosfatos de calcio bifásicos bien cristalizados en una sola etapa mediante la técnica de combustión de soluciones y con respuesta antimicrobiana, un hecho que puede significar la reducción del coste de producción de estos materiales. Los difractogramas de rayos X evidenciaron que los polvos preparados presentaron una alta cristalinidad debido a las altas temperaturas durante la reacción de combustión. El refinamiento Rietveld mostró que la inclusión de las nanopartículas de oro influenciaron la relación de las fases obtenidas. La microscopia electrónica de barrido mostró la aglomeración de partículas con morfologías tendentes a ser equigranulares. La presencia de nanopartículas de oro fue corroborada mediante microscopia electrónica de transmisión. Todas las muestras que fueron obtenidas en un solo paso mediante la combustión de soluciones mostraron un comportamiento antimicrobiano validado a través de halos de inhibición, mientras que, en las partículas sometidas a tratamiento térmico, este comportamiento estuvo ausente.

Introduction

The most widely inorganic biomaterials used in applications of bone tissue engineering, like medical implants, are calcium phosphates (CP) mainly for their biocompatibility and similarity with the inorganic phase present in the bone [1]. The main phases of CP with applications in the design of implants are hydroxyapatite (HA) [2,3], tricalcium phosphates (TCP) [4,5], and biphasic calcium phosphates (BCPs) [6], every one holds different properties and performance. The BCPs are the mixture of HA and beta-tricalcium phosphates (β-TCP) in different weight-in-weight (w/w) ratios for HA/β-TCP. These materials are very interesting due to both their bioreapsortion and bioactivity properties. Depending on the change in these ratios, different scaffold behaviors can be obtained [7]. The most frequent complications associated with biomaterials used in the development of medical implants are failures owing to bacterial colonization or infectious diseases. Furthermore, in recent years the emergence of antibiotic-resistant bacteria and fungi makes infectious diseases a dangerous public health problem [8]. Therefore, searching for new antibiotics or therapies to treat diseases and avoid implant failure is paramount. Recently, a strategy to avoid bacterial colonization in implants, is the incorporation of antimicrobial agents different from traditional antibiotics like antimicrobial peptides, enzymes, polymers, metal, and ceramic nanoparticles. AuNPs is an attractive choice, on account of its high stability, antimicrobial, photothermal, catalytic activity, etc [3,9,10]. The typical antimicrobial activity of Au nanoparticles is related to oxidative stress induction by producing reactive oxygen species and non-oxidative stress mechanisms such as membrane potential modification, Adenosine triphosphate level decrease and inhibition of Transfer ribonucleic acid binding to the ribosome, that could kill Gram-positive and Gram negative bacteria [11–13]. For this reason, the combination of calcium phosphates with Au could be used to obtain different structures with antimicrobial behavior. Different research has been carried out on this topic, mainly on the effect of doping on the structures of HAP and TCP, but little information has been reported on the inclusion of gold nanoparticles directly in biphasic calcium phosphates. Banerjee et al. synthesized porous HAP pellets impregnated with gold nanoparticles, obtaining HAP by co-precipitation method and a thermal treatment to 650 °C first, and subsequently combined with gold nanoparticles synthesized by reduction. The samples showed strong antimicrobial activity against *Escherichia coli* and *Staphylococcus aureus* [9]. Mondal et al. and Nirmala et al. obtained a HAP-Au composite using HAP synthesized using the precipitation method and gold colloid. The HAP-Au composite showed low crystallinity and broad spectrum antibacterial activity [11,14]. Yang Xia et al. [15] obtained a composite cement of calcium phosphates – AuNPs, by means of solid state reaction of calcium phosphates, tetracalcium phosphate (TTCP) and anhydrous dicalcium phosphate (DCPA). The inclusion of AuNPs into the calcium phosphates scaffold enhanced the osteogenic differentiation of dental pulp stem cells, thus showing great potential to improve bone regeneration [15]. Solution combustion synthesis is a process that allows obtaining ceramic powders without the need for calcination, which generates energy saving in the process, since during synthesis there is a self-sustained high-temperature combustion reaction, given

that the precursors of the desired phase are a fuel and an oxidant; additionally, the powders have primary particle sizes of less than 100 nm [16]. Solution combustion has been used to synthesize powders with applications such as pigments, magnetic materials, catalysts, lithium ion batteries, among others [17–20]. In the last decade, there has been a great interest in the synthesis of calcium phosphates using solution combustion synthesis, where studies on the effect of the synthesis parameters such as fuel type, pH, oxidizer/fuel ratio in obtaining the hydroxyapatite and tricalcium phosphates phases, as well as their influence on the powder microstructure, has also been considered for applications in bioceramics [21–23]. To date, no reports have yet been found on the synthesis of composites between bicalcium phosphates and gold using solution combustion synthesis with potential antimicrobial application.

This work aimed at obtaining gold nanoparticles supported on BCPs with high crystallinity by, in one step, using solution combustion technique. Also, morphological, structural characterization, and antimicrobial response of composite was carried out to validate the potential applications in antimicrobial bone tissue engineering.

Experimental procedure

Structural and morphological characterization of samples

Biphasic calcium phosphates/AuNPs nanocomposites were obtained by, in one-step, using a solution combustion method. Calcium nitrate tetrahydrate ($Ca(NO_3)_2{\cdot}4H_2O$) was used like oxidant (O), glycine ($C_2H_5NO_2$) was used as a fuel (F) and diammonium hydrogen phosphate ($(NH_4)_2HPO_4$) (DHP) as a phosphate precursor. Solutions of calcium- phosphates were prepared. First, the DHP and calcium nitrate were mixed in distilled water under magnetic stirring at room temperature in a proportion Ca:P = 1.5 forming a precipitate subsequently dissolved with nitric acid (HNO_3). The fuel was added in oxidizer-to-fuel ratio O/F = 1 [24]; this solution was called SA. Monodisperse AuNPs solutions nanoparticles were obtained by means of chloroauric acid reduction to metallic gold. In this case, a mixture of 150 mL of sodium citrate (2.2 mM) with 0.1 mL of tannic acid (2.5 mM), were heated with continuous stirring at 70 °C, at pH 8. Then, 1 mL of chloroauric acid ($HAuCl_4$ 25 mM) was injected into the solution. Thus, the solution turned from transparent to dark gray first, and to dark red later, indicating gold nanoparticles formation. The AuNPs were mixed with the SA solution in different AuNPs concentration (% by weight referring to the content of BCPs) 0.2%, 0.7%, 1%, 2%, 4%, 9%, respectively. The final solution was maintained at approximately 80 °C under stirring until a gel appeared. Then the temperature of the gel was increase at 200 °C–250 °C until gel ignition. Part of the powders obtained after combustion were thermal treated at 800 °C for two hours to increase crystallinity and eliminate the possible residual organic matter from the combustion.

The crystalline structures of the samples were identified using data from a D8 Advance Eco Bruker model diffractometer from Bruker (Karlsruhe, Germany). The refinements using the Rietveld method were performed using Topas Academic V5 [25] software through the fundamental parameters to adjust peak shapes. Fourier transform infrared spectroscopy (FTIR) analyses were made on a Nicolet Magna IR 550 Spectrometer Series II. The Size and morphology of sample particles were observed with a scanning electron microscope (SEM, EVO MA10 Carl Zeiss microscope) and transmission electron microscope (Tecnai F20 Super Twin TMP de FEI) the images were processed for grain size measurement using ImageJ software. Simultaneous differential scanning calorimeter and thermogravimetric analysis (DSC/TGA, TA Instruments – Discovery SDT 650) were employed to investigate the processes of gel combustion.

Antimicrobial assay

The antimicrobial activity of the samples was tested using *S. aureus* (ATCC®29213™). The bacterial inoculum was initially seeded in Luria–Bertani (LB) broth nutrient, and then subcultured on a petri dish. The cultured dishes were placed inside the incubator with temperature set at 37 °C for 12 h. Discs of 8 mm diameter, 2 mm thick previously sterilized were placed in the center of petri dish and maintained at 37 °C for 18 h. The experimental study was conducted in duplicate; after that, each plate was examined and the presence of colonies grown on the material surface or the inhibition halos (zone of inhibition) was visualized and measured using a caliper. Ciprofloxacin was used as control.

Results and discussion

The simultaneous DSC/TGA results of the gel are shown in Fig. 1. The weight loss in the range of 100 °C–200 °C is very likely due to dehydration and partial thermal decomposition of precursors [26]. After 200 °C a multi-step exothermic decomposition was observed for the three concentrations of AuNPs, the first exothermic behavior of auto-ignition can be clearly seen about 210 °C, the weight loss associated with this peak in the samples was 33%, 38% and 29% respectively. While the weight loss associated with the exothermal second peak was 6%, 15% and 20% Similar results of a multi-step combustion have been previously observed by Purohit et al. in the glycine-nitrates system [27]. The broad peak in the DSC between 260 and 550 °C corresponds to removing residual organic material due to the incomplete combustion process with the weight loss of 15%, 15% and 4% respectively, these results could indicate that increasing the gold nanoparticles in the gel, the second step combustion is favored together with complete combustion (Fig. 1c). The combustion solution has been understood as an exothermic reaction resulting from the redox reaction between the ions present in the gel in the form of complexes [24]. In some way, the presence of the AuNPs solution could favor combustion at higher temperatures. However, the combustion mechanisms for each mixture of ions or complexes are not yet fully understood, and further studies should be conducted around this.

Fig. 2 shows the Rietveld plot of the target of the BCPs powders with thermal treatment (TT) which were compared with JCPDS cards and for the samples analyzed three phases were identified, JCPDS #86-1199 for the hydroxyapatite, JCPDS #29-359 for the alpha-tricalcium phosphate and JCPDS #70-2065

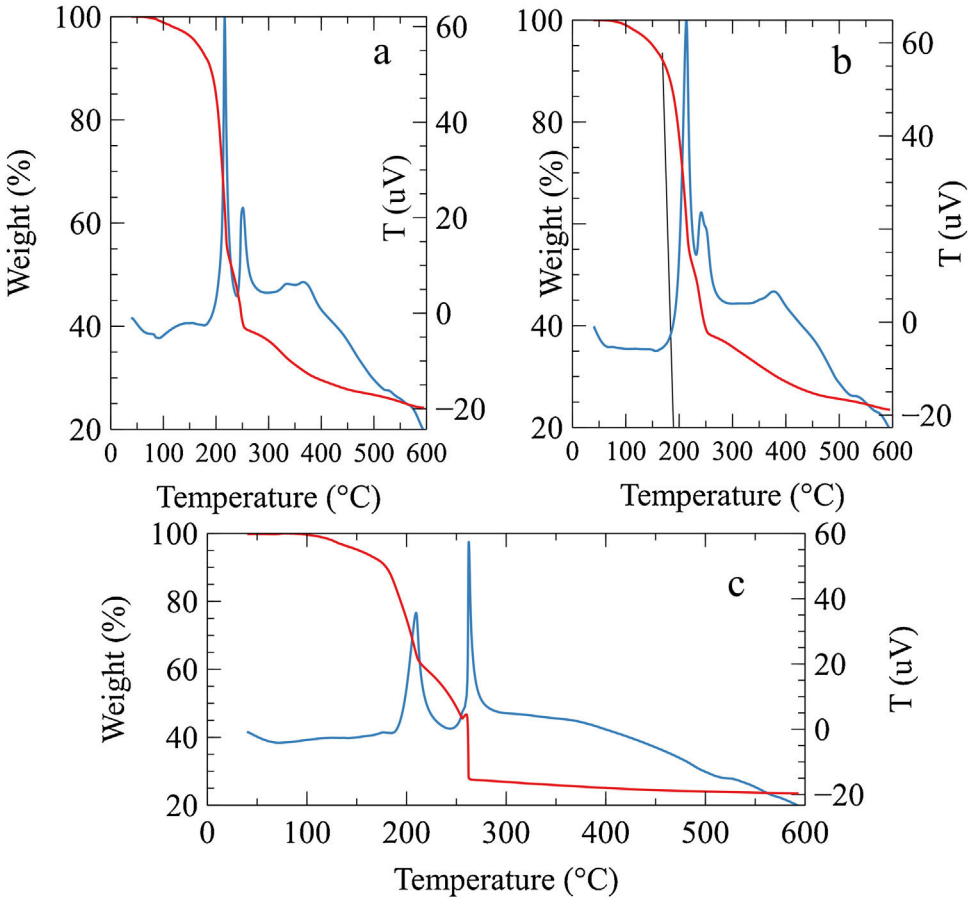

Fig. 1 – DSC/TGA of the gel after of combustion: (a) BCPs Gel, (b) Gel 1% Au and (c) Gel 9% Au.

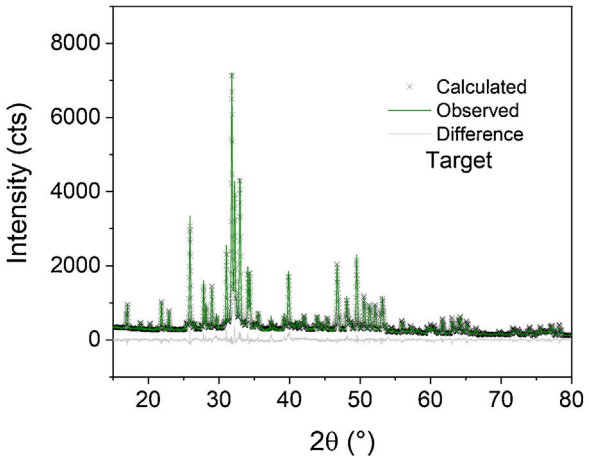

Fig. 2 – Rietveld plot for the Target sample BCPs with TT and without AuNPs.

for the beta-tricalcium phosphate. The crystal structures used to perform the refinements were obtained from the Inorganic Crystal Structure database (ICSD) under codes 56306, 923 and 97500, respectively. The Rietveld plot of the refinements performed for the BCPs samples with Au are presented in Fig. 3. All the patterns showed well-adjusted profiles between the observed and calculated diffractograms, as can be seen in the figure. The 2%, 4% and 9% plots and the agreement factors for the refinements (table S1) are presented in the supplementary material. Comparing the BCPs-Au samples with the target sample (Fig. 2) it is possible to observe that the high crystallinity is preserved although the phase amount varies for each sample.

Table 1 shows the lattice parameters obtained through refinement of target sample and the one that contained the greatest amount of Au (9%). As can be seen, the lattice parameters obtained for the phases present in the samples oscillate within the calculated deviations, which shows that they do not vary significantly when compared to the samples at both ends, i.e., without Au addition and with the greatest Au concentration. This indicates that Au was not incorporated into crystal structure, maintaining them as in the pure phase (target).

It is worth noting that, although Au was not incorporated in the crystal structures, the variation of the amounts of calcium phosphate phases may be related to an influence of nanoparticles dispersion on the homogeneity of combustion temperature through the solution (Fig. 4a and b). It is likely that with the inclusion of AuNPs certain regions, some rich in fuels and others poor, are generated. Samir Kumar et al. [26] reported that with the variation of the oxidizing fuel ratio the theoretical temperatures can vary from 847 °C to 1531 °C, in such a way that in some cases the formation of higher temperature phases will be favored, and in others, the exact opposite will occur. Besides, the dehydration processes are activated as

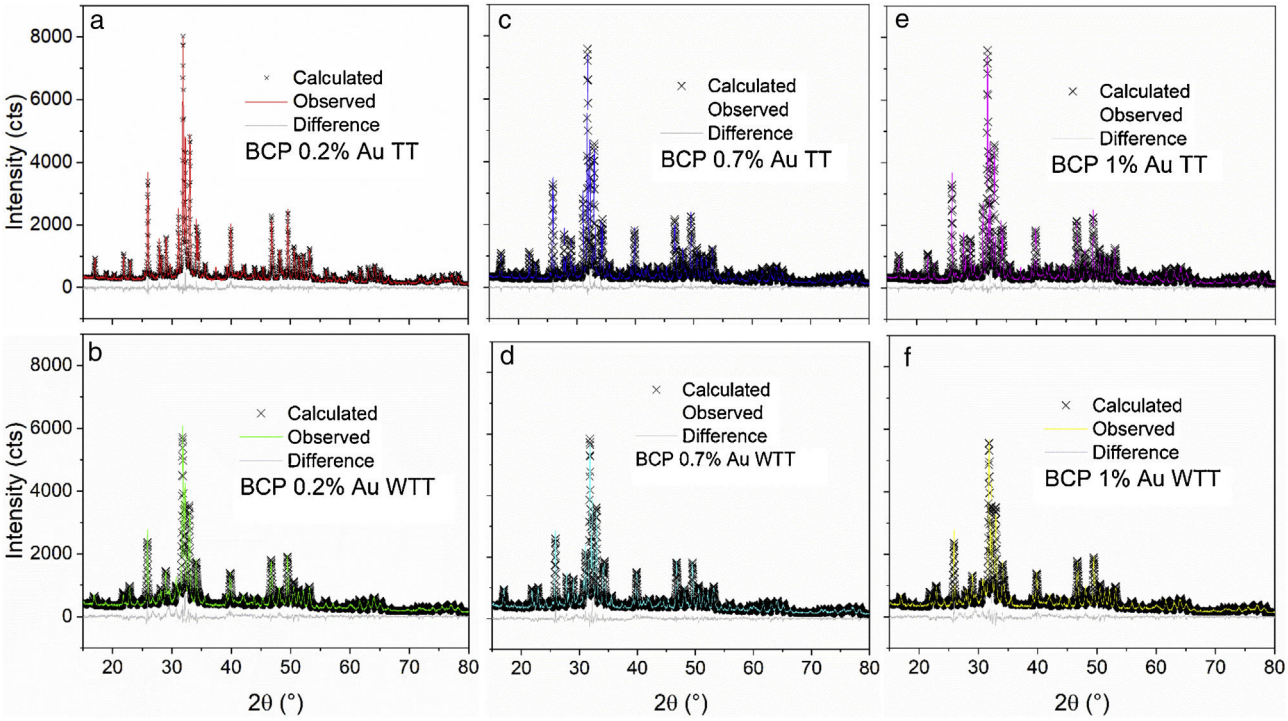

Fig. 3 – Rietveld plots of BCPs–AuNPs samples: (a) 0.2% TT (TT = thermal treatment), (b) 0.2% WTT (WTT = without thermal treatment), (c) 0.7% TT, (d) 0.7% WTT, (e) 1% TT, (f) 1% WTT.

Table 1 – Refinement data for the Target (top) and the greatest Au content (bottom) without thermal treatment samples.

Lattice (Å)	Target (Rwp = 7.87%, gof = 1.61)			Au 9%(Rwp = 8.75%, gof = 1.84)		
	HA	α-TCP	β-TCP	HA	α-TCP	β-TCP
a	9.4203(1)	12.96(4)	10.4411(3)	9.4292(4)	12.861(4)	10.4466(9)
b	9.4203(1)	27.32(6)	10.4411(3)	9.4292(4)	27.354(4)	10.4466(9)
c	6.8880(1)	15.12(2)	37.416(1)	6.8916(4)	15.215(2)	37.331(5)
β		125.9(2)			126.29(2)	
Vol (Å^3)	529.36(2)	4336(20)	3532.5(3)	530.65(6)	4314(2)	3528.1(8)
R_{Bragg}	2.52	3.55	3.56	3.05	4.35	4.05
wt%	77.5(4)	1.7(4)	20.8(3)	73.3(5)	15.0(3)	11.8(4)

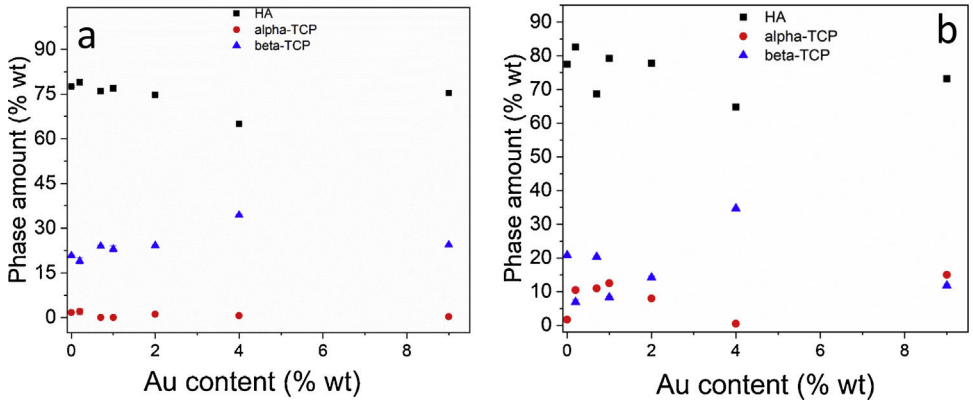

Fig. 4 – Phases amount in weight proportion (wt%) for samples (a) with thermal treatment; (b) without thermal treatment.

the temperature is increased. So, if the stoichiometric Ca/P ratio decreases to 1:5, the formation of TCP is favored. For ratios Ca/P greater than 1.67 there are energy barriers that limit the incorporation of hydroxyl groups in the structure [28]. Previous work [29] has shown that when calcium phosphates are obtained through the combustion route and submitted to

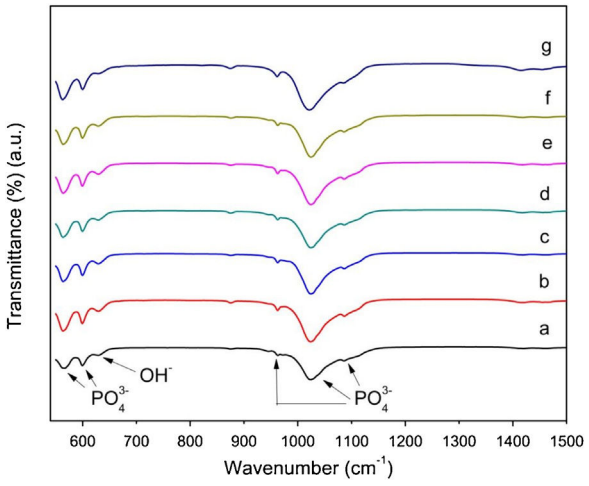

Fig. 5 – FTIR spectra of BCPs–AuNPs samples: (a) 0.2% WTT, (b) 0.2% TT, (c) 1% WTT, (d) 1% TT, (e) 4% WTT, (f) 4% TT, (g) BCPs TT.

thermal treatment, the beta phases increase, while the alpha phase decreases. A similar effect occurred in this case when comparing Fig. 3a and b.

Fig. 5, shows the FTIR spectra of the powders, which reveal the presence of the characteristic vibration modes of phosphate groups with bands at 563 and 602 cm^{-1}, which are attributed to P–O bending vibration mode of the phosphate group PO_4^{3-}. Moreover, bands at 961, 1023, and 1086 cm^{-1} can be assigned to symmetric vibration of stretching in PO_4^{3-}. On the other hand, there is a band at 632 cm^{-1} which corresponds to OH– stretching vibration. The presence of these bands is in agreement with previous reports and confirms the formation of calcium phosphates without evidencing changes associated with AuNPs inclusion.

TEM and size distribution of the synthesized gold nanoparticles are presented in Fig. 6a and b. Homogeneous distribution of the particles with spherical morphologies and size around 4 nanometers are observed. Absorbance peak around 536 nm is indicative of gold nanoparticles formation (surface Plasmon absorption band) [9].

Fig. 7 shows SEM images of calcium phosphates with impregnated AuNPs – WTT (a–c) and without AuNPs – WTT (d). In the samples synthesized with AuNPs, the aggregate distribution appears to have a bimodal distribution, the first between 10 μm and 100 μm and the second 1 μm–10 μm. In the samples synthesized with AuNPs, it was possible to identify two types of morphologies in aggregates formation: one tending to be granular and the other with the form of flower or plates (Fig. 7a–c). While this type of double morphology is not observed in the synthesized particles without the presence of AuNPs (Fig. 7d). In this case, it is only likely to identify aggregate with granular forms and some of them have sizes greater than two microns. In the combustion reactions resulting from reactant decomposition and exothermic reaction, spontaneous nucleation and growth occur. Aggregates formation by traditional combustion synthesis is due to the temperature reached during the reaction and the release of gases [30]. In general, at a higher combustion temperature with less gas release, the formation of more significant aggregates is favored along with a larger particle grain size. Combustion temperature is influenced by the fuel/oxidizer ratio. In this work the relation was $\Phi = 1$. This value allows obtaining a theoretical complete combustion reaction reaching the maximum heat combustion, which agrees with Fig. 6c, where it is possible to observe that the growth processes, agglomeration, and sintering of grains were favored. Conversely, in the samples where the suspension of gold nanoparticles was added in the synthesis, an influence on the morphology was observed. This effect can be related to an alteration in the reaction conditions of the combustion complexes generating a greater release of gases and a possible decrease in flame temperature compared to the sample without nanoparticles. Similar results are found in combustion reactions in which, by adding different additives, it is possible to control morphological properties [31].

TEM images of BCPs particles with and without AuNPs (Fig. 8a–d) showed that the aggregates were composed of grains of near-spherical or irregular isotropic morphology

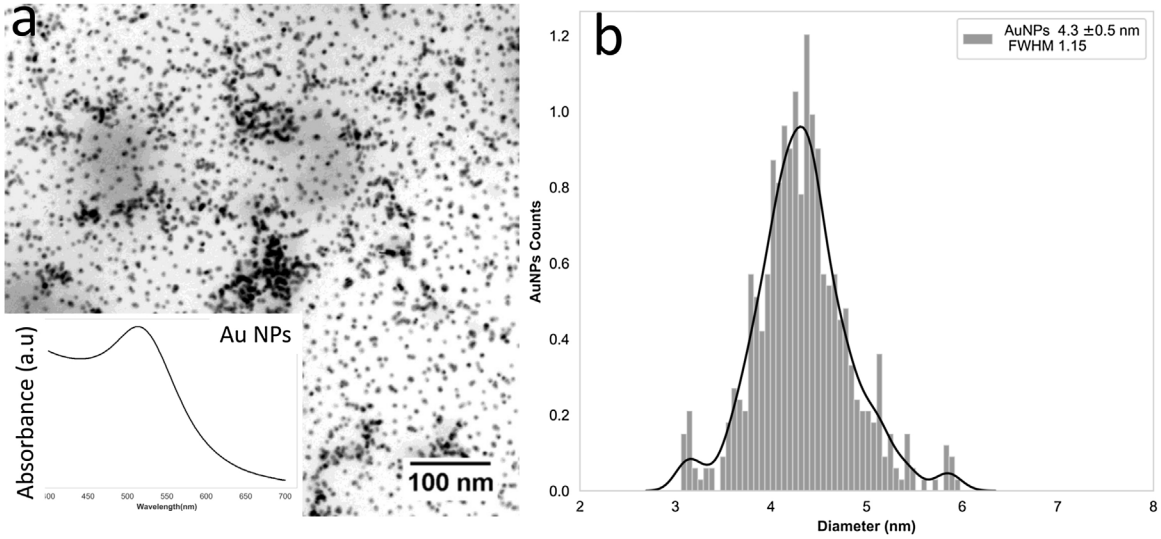

Fig. 6 – (a) TEM Au nanoparticles and (b) AuNPs size distribution.

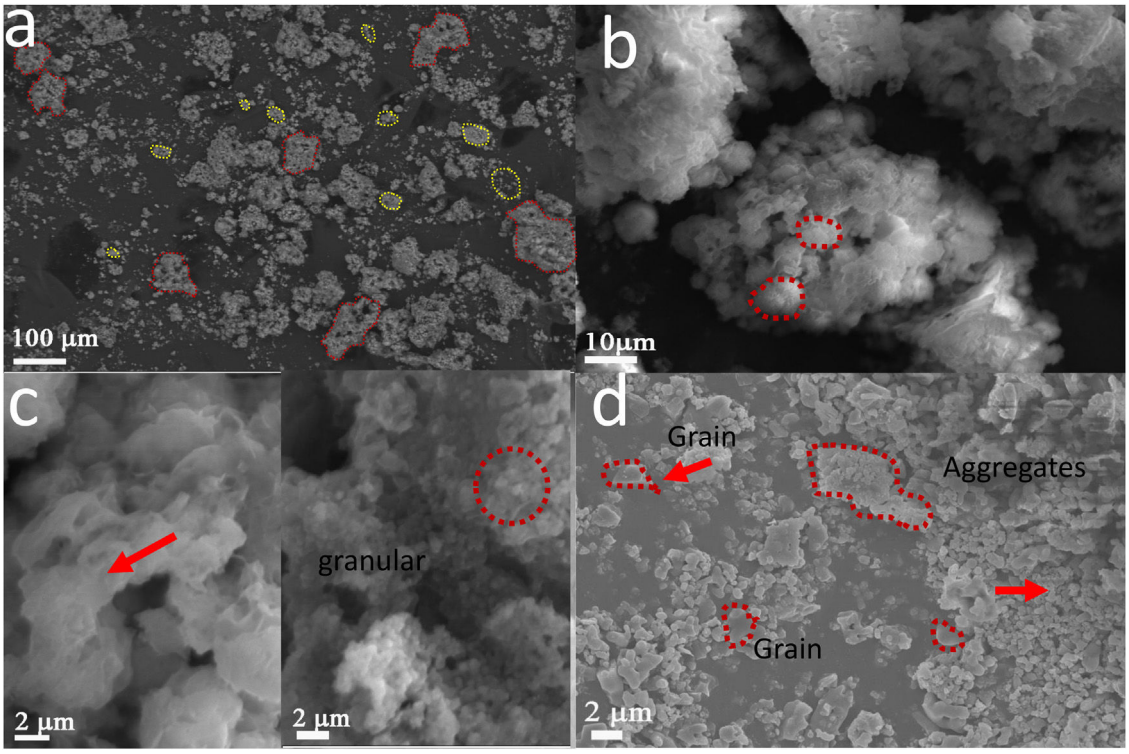

Fig. 7 – (a–c) Powder of BCPs samples with AuNPs-WTT and (d) BCPs without AuNPs-WTT.

with an important account of pores with average diameter 12 nm ± 7 nm. The statistical analyze of the images showed a grain size of approximately 67 nm ± 26 nm both for phosphates with and without AuNPs (Fig. 8a and b). The porous could be because of the release of gases during combustion. In Fig. 8c, it can be observed spherical and monodispersed AuNPs with different size particle (black particles). The difference in size particle could be attributed to the reaction conditions during combustion synthesis. A possible agglomeration of AuNPs during the solvent evaporation until the gel formation and subsequently the growth of grain influenced by the temperatures reached during the gel combustion. Fig. 8d–e shows that some smallest metal particles were embedded in the porous microstructure, while some largest metal particles were supported on the surface of BCPs. This effect corroborates the capability of these structures obtained by combustion to be used as potential encapsulation and support systems for various nanoparticles. Fig. 8f shows a high-resolution TEM image of a gold nanoparticle without thermal treatment in which the d_{111} crystalline plane of the AuNPs nanoparticles is identified, corroborating that the black spots in the photos are the AuNPs. Through thermal treatment of BCPs–AuNPs the black spots disappear (Fig. 8g) but the presence of crystalline plane indicates the presence of Au d_{111} and d_{112} (Fig. 8h).

The ability of BCPs–AuNPs nanostructures against *S. aureus* was studied. Fig. 9 shows the ability of various BCPs–AuNPs restricting the growth of *S. aureus*. The zone of inhibition measured in diameter (mm) around the BCPs disc against the analyzed strains revealed that the BCPs–AuNPs WTT showed a very good antimicrobial effect compared to the control (Fig. 9d–g), while the BCPs–AuNPs TT did not show antimicrobial behavior (Fig. 9a–c). As the gold content is increased, the inhibition percentage increases, i.e. with 9% Au the inhibition percentage was 78%, Table 2.

As mentioned above, the antibacterial response of gold nanoparticles is mainly related to particle size, and its relation with the ability to introduce into the cell or associate with the membrane, causing different damages, either by direct mechanisms such as oxidative stress or indirect as the modification of membrane potential. These results are associated with the presence of supported gold nanoparticles in the BCPs. As the concentration of the AuNPs solution was increased, a greater distribution of nanoparticles was observed in the BCPs. Whereas, when the calcium phosphates are treated with thermal treatment (800 °C), their antimicrobial capacity disappear, this can be associated with gold nanoparticle degradation resulting from the nucleation and growth phenomena that can occur during the increase in temperature (over 600 °C). Different investigations have reported the stability of supported gold nanoparticles in calcium phosphates like HAP but only 600 °C. i.e. Wang et al. found that the stabilized gold nanoparticles depend on phosphates groups for temperatures below 400 °C and the hydroxyl groups to higher temperatures (below 600 °C) [32]. It is important to note that the theoretical temperature of redox reaction during combustion synthesis is around 1035 °C [26] but the times of reaction are very short so the kinetic of reaction is not enough to produce destabilization of gold nanoparticles.

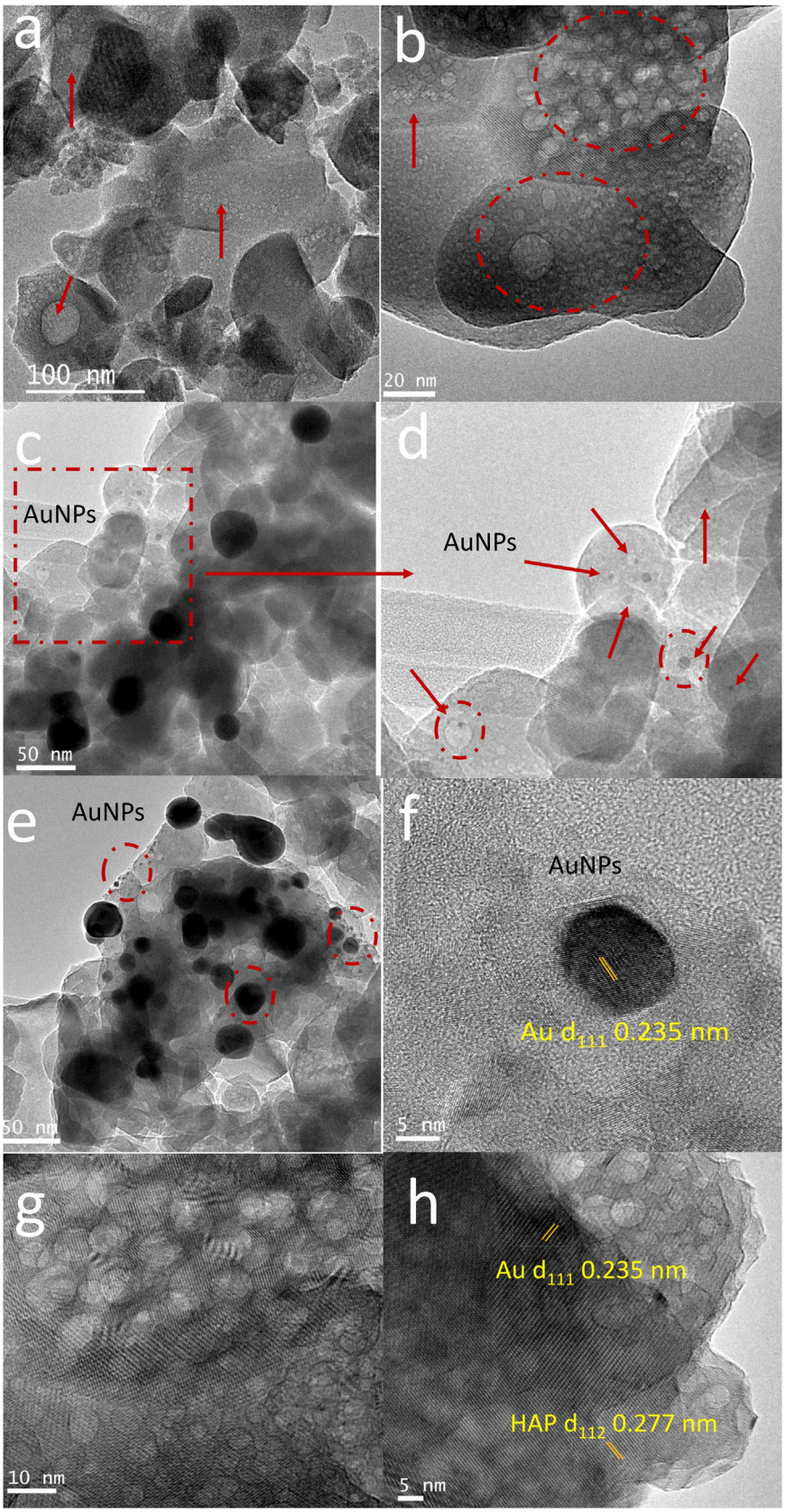

Fig. 8 – TEM of BCPs–AuNPs powders (a and b) BCPs without AuNPs-WTT, (c and d) BCPs–AuNPs WTT and (e and f) BCPs–AuNPs TT at 800 °C 2 h.

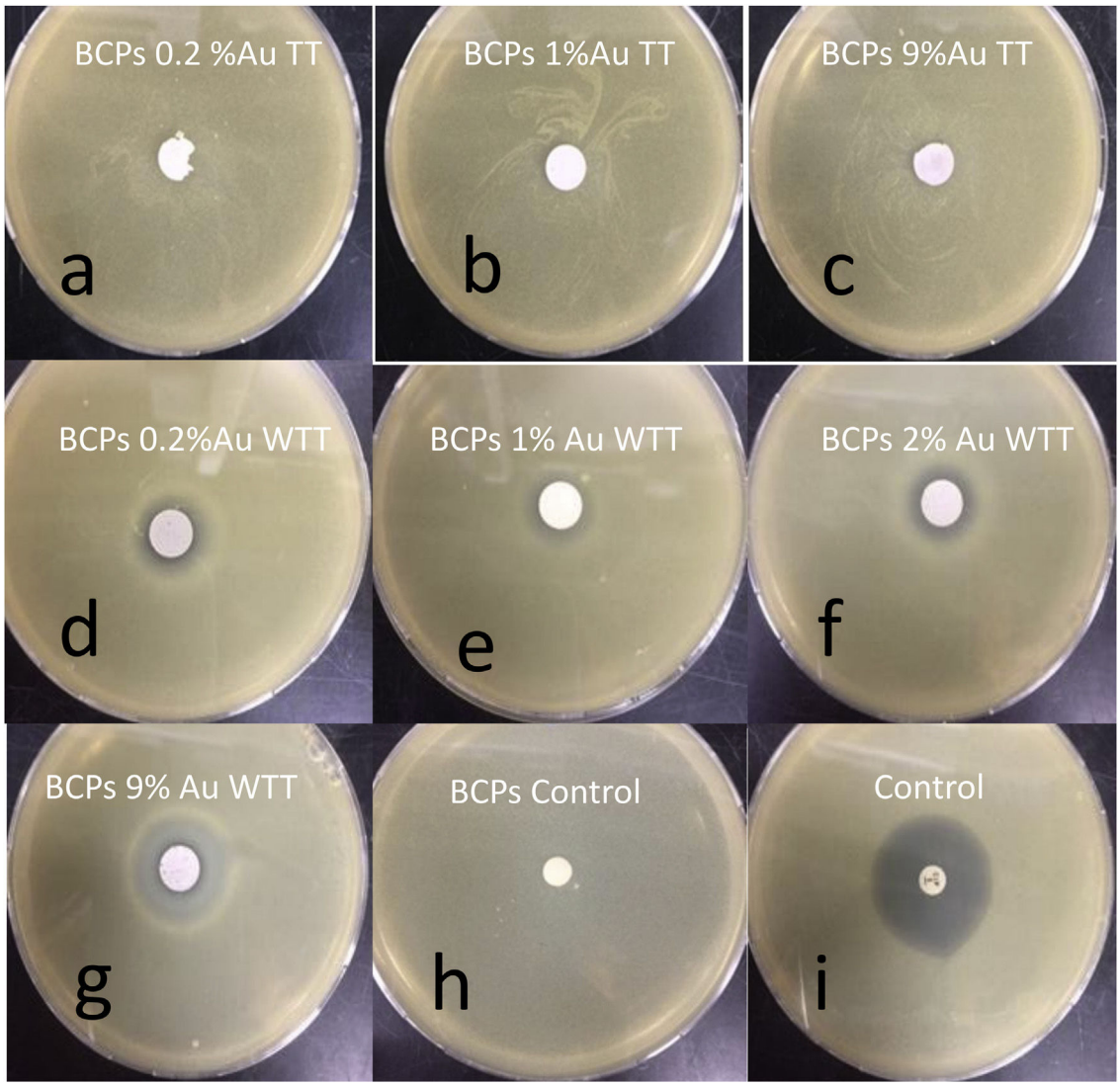

Fig. 9 – Inhibition halos obtained after co-cultivation of *S. aureus* with the BCPs–AuNPs and controls: (a–c) BCPs–AuNPs TT, (d–g) BCPs–AuNPs WTT and (h and i) control.

Table 2 – Inhibition percentages of BCPs–AuNPs WTT.

Sample	Inhibition halo (diameter-mm)	% Inhibition halo/control
BCPs 0.2% Au	13.4 ± 0.2	37
BCPs 0.7% Au	15.4 ± 1.3	42
BCPs 1% Au	11.4 ± 0.4	31
BCPs 2% Au	15.2 ± 0.6	42
BCPs 4% Au	17.9 ± 0.6	49
BCPs 9% Au	28.2 ± 3.0	78
BCPS negative control	0	0
Positive control	36.4 ± 0.4	NA

Conclusion

BCPs/AuNPs composites were synthesized in a one-step by hybrid combustion synthesis, using glycine as fuel and gold nanoparticles suspension. The conventional synthesis of Au nanoparticles allowed obtaining particles with spherical morphology and adequate dispersion, the media value of nanoparticle size was 4.3 nm. XRD showed that biphasic calcium phosphates were obtained with high crystallinity even without thermal treatment. The presence of Au nanoparticles was corroborated by TEM microscopy, where it was possible to see an increase in the size grain of gold nanoparticles. Moreover, the biphasic calcium phosphates showed the presence of porosity in the grains where gold particles were housed. SEM microscopy revealed that the morphology of the particles is granular and the other type flower or plates. These results are directly related to the conditions of combustion synthesis reaction. There is a strong relationship between temperature and gas release with structural and morphological properties. Antimicrobial tests revealed that the phosphates containing AuNPs obtained directly from the combustion reaction exhibited adequate antimicrobial behavior against *S. aureus*, while the antimicrobial behavior disappears with thermal treatment, possibly due to the destabilization of the nanoparticles. These results enhance the possibility of using the

combustion in solution route to obtain calcium phosphate compounds with antimicrobial response even reducing costs by not having to thermally treat the products after reaction.

Acknowledgements

Authors are very grateful to "Convocatoria Colciencias No. 784 de Estancias Posdoctorales" - Minciencias.

Appendix A. Supplementary data

Supplementary data associated with this article can be found, in the online version, at doi:10.1016/j.bsecv.2021.03.007.

REFERENCES

[1] I. Denry, L.T. Kuhn, Design and characterization of calcium phosphate ceramic scaffolds for bone tissue engineering, Dent. Mater. 32 (2016) 43–53, http://dx.doi.org/10.1016/j.dental.2015.09.008.
[2] S. Mondal, U. Pal, 3D hydroxyapatite scaffold for bone regeneration and local drug delivery applications, J. Drug Deliv. Sci. Technol. 53 (2019) 101131, http://dx.doi.org/10.1016/j.jddst.2019.101131.
[3] H. Kim, S. Mondal, B. Jang, P. Manivasagan, M.S. Moorthy, J. Oh, Biomimetic synthesis of metal–hydroxyapatite (Au-HAp, Ag-HAp, Au-Ag-HAp): structural analysis, spectroscopic characterization and biomedical application, Ceram. Int. 44 (2018) 20490–20500, http://dx.doi.org/10.1016/j.ceramint.2018.08.045.
[4] R.G. Carrodeguas, S. De Aza, α-Tricalcium phosphate: synthesis, properties and biomedical applications, Acta Biomater. 7 (2011) 3536–3546, http://dx.doi.org/10.1016/j.actbio.2011.06.019.
[5] T. Tanaka, H. Komaki, M. Chazono, S. Kitasato, A. Kakuta, S. Akiyama, K. Marumo, Basic research and clinical application of beta-tricalcium phosphate (β-TCP), Morphologie 101 (2017) 164–172, http://dx.doi.org/10.1016/j.morpho.2017.03.002.
[6] J.M. Bouler, P. Pilet, O. Gauthier, E. Verron, Biphasic calcium phosphate ceramics for bone reconstruction: a review of biological response, Acta Biomater. 53 (2017) 1–12, http://dx.doi.org/10.1016/j.actbio.2017.01.076.
[7] M. Ebrahimi, M.G. Botelho, S.V. Dorozhkin, Biphasic calcium phosphates bioceramics (HA/TCP): concept, physicochemical properties and the impact of standardization of study protocols in biomaterials research, Mater. Sci. Eng. C 71 (2017) 1293–1312, http://dx.doi.org/10.1016/j.msec.2016.11.039.
[8] X. Ge, Antimicrobial biomaterials with non-antibiotic strategy, Biosurf. Biotribol. 5 (2019) 71–82.
[9] S. Banerjee, B. Bagchi, S. Bhandary, A. Kool, N. Amin Hoque, P. Thakur, S. Das, A facile vacuum assisted synthesis of nanoparticle impregnated hydroxyapatite composites having excellent antimicrobial properties and biocompatibility, Ceram. Int. 44 (2018) 1066–1077, http://dx.doi.org/10.1016/j.ceramint.2017.10.051.
[10] S.M. Dizaj, F. Lotfipour, M. Barzegar-Jalali, M.H. Zarrintan, K. Adibkia, Antimicrobial activity of the metals and metal oxide nanoparticles, Mater. Sci. Eng. C 44 (2014) 278–284, http://dx.doi.org/10.1016/j.msec.2014.08.031.
[11] R. Nirmala, H.-M. Park, D. Kalpana, H.-S. Kang, R. Navamathavan, Y.-S. Lee, H.Y. Kim, Bactericidal activity and in vitro cytotoxicity assessment of hydroxyapatite containing gold nanoparticles, J. Biomed. Nanotechnol. 7 (2011) 342–350.
[12] Y.-T. Huang, Y. Yamauchi, C.W. Lai, W.J. Chen, Evaluating the antibacterial property of gold-coated hydroxyapatite: a molecular biological approach, J. Hazard. Mater. 277 (2014) 20–26.
[13] Y. Cui, Y. Zhao, Y. Tian, W. Zhang, X. Lü, X. Jiang, The molecular mechanism of action of bactericidal gold nanoparticles on *Escherichia coli*, Biomaterials 33 (2012) 2327–2333, http://dx.doi.org/10.1016/j.biomaterials.2011.11.057.
[14] S. Mondal, G. Hoang, P. Manivasagan, M.S. Moorthy, T.T.V. Phan, H.H. Kim, T.P. Nguyen, J. Oh, Rapid microwave-assisted synthesis of gold loaded hydroxyapatite collagen nano-bio materials for drug delivery and tissue engineering application, Ceram. Int. 45 (2019) 2977–2988.
[15] Y. Xia, H. Chen, F. Zhang, C. Bao, M.D. Weir, M.A. Reynolds, J. Ma, N. Gu, H.H.K. Xu, Gold nanoparticles in injectable calcium phosphate cement enhance osteogenic differentiation of human dental pulp stem cells, Nanomed. Nanotechnol. Biol. Med. 14 (2018) 35–45, http://dx.doi.org/10.1016/j.nano.2017.08.014.
[16] H.H. Nersisyan, J.H. Lee, J.R. Ding, K.S.K. Kim, V. Manukyan, A.S. Mukasyan, Combustion synthesis of zero-, one-, two- and three-dimensional nanostructures: current trends and future perspectives, Prog. Energy Combust. Sci. 63 (2017) 79–118, http://dx.doi.org/10.1016/j.pecs.2017.07.002.
[17] D.G. Kuvshinov, P.B. Kurmashov, A.G.M. Bannov, V. Popov, G.G. Kuvshinov, Synthesis of Ni-based catalysts by hexamethylenetetramine-nitrates solution combustion method for co-production of hydrogen and nanofibrous carbon from methane, Int. J. Hydrogen Energy 44 (2019) 16271–16286, http://dx.doi.org/10.1016/j.ijhydene.2019.04.179.
[18] S. Golchinvafa, S.M. Masoudpanah, Magnetic and microwave absorption properties of $FeNi_3$/$NiFe_2O_4$ composites synthesized by solution combustion method, J. Alloys Compd. 787 (2019) 390–396, http://dx.doi.org/10.1016/j.jallcom.2019.02.039.
[19] Y. Zhang, P. Dong, J. Zhao, X. Li, Y. Zhang, Simple solution-combustion synthesis of Fe_2TiO_5 nanomaterials with enhanced lithium storage properties, Ceram. Int. 45 (2019) 11382–11387, http://dx.doi.org/10.1016/j.ceramint.2019.03.002.
[20] N. Vollmer, R. Ayers, Decomposition combustion synthesis of calcium phosphate powders for bone tissue engineering, Int. J. Self-Propagat. High-Temp. Synth. 21 (2012) 189–201, http://dx.doi.org/10.3103/S1061386212040073.
[21] M.A. Aghayan, M.A. Rodríguez, Influence of fuels and combustion aids on solution combustion synthesis of bi-phasic calcium phosphates (BCP), Mater. Sci. Eng. C 32 (2012) 2464–2468, http://dx.doi.org/10.1016/j.msec.2012.07.027.
[22] J. Zhao, J. Zhao, Y. Qian, X. Zhang, F. Zhou, H. Zhang, H. Lu, J. Chen, X. Wang, W. Yu, Solution combustion synthesis of calcium phosphate particles for controlled release of bovine serum albumin, Mater. Sci. Eng. C 50 (2015) 194–200, http://dx.doi.org/10.1016/j.msec.2015.02.006.
[23] D. Bovand, A.M. Arabi, M. Bovand, Microwave assisted solution combustion synthesis of β-tricalcium phosphate nano-powders, Bol. La Soc. Esp. Ceram. Vidr. 57 (2018) 240–246, http://dx.doi.org/10.1016/j.bsecv.2018.05.001.
[24] K.C. Patil, Chemistry of Nanocrystalline Oxide Materials: Combustion Synthesis, Properties and Applications, World Scientific, 2008.
[25] A.A. Coelho, TOPAS and TOPAS-Academic: an optimization program integrating computer algebra and crystallographic objects written in C++, J. Appl. Crystallogr. 51 (2018) 210–218.

[26] S.K. Ghosh, S.K. Roy, B. Kundu, S. Datta, D. Basu, Synthesis of nano-sized hydroxyapatite powders through solution combustion route under different reaction conditions, Mater. Sci. Eng. B 176 (2011) 14–21, http://dx.doi.org/10.1016/j.mseb.2010.08.006.
[27] R.D. Purohit, S. Saha, A.K. Tyagi, Nanocrystalline thoria powders via glycine-nitrate combustion, J. Nucl. Mater. 288 (2001) 7–10.
[28] N. Eliaz, N. Metoki, Calcium phosphate bioceramics: a review of their history, structure, properties, coating technologies and biomedical applications, Materials (Basel) 10 (2017) 334.
[29] A.A. Lopera, E.A. Chavarriaga, B. Zuluaga, S. Marin, G.O. Giraldo, H.A. Estupiñan, V. Zapata, C.P. Garcia, Effect of salt concentration on the electrical and morphological properties of calcium phosphates obtained via microwave-induced combustion synthesis, Adv. Powder Technol. 28 (2017) 2787–2795, http://dx.doi.org/10.1016/j.apt.2017.08.007.
[30] K.C. Patil, S.T. Aruna, T. Mimani, Combustion synthesis: an update, Curr. Opin. Solid State Mater. Sci. 6 (2002) 507–512, http://dx.doi.org/10.1016/S1359-0286(02)00123-7.
[31] A.K. Alves, C.P. Bergmann, F.A. Berutti, Novel Synthesis and Characterization of Nanostructured Materials, Springer, 2013.
[32] Y. Wang, B. Chen, M. Crocker, Y. Zhang, X. Zhu, C. Shi, Understanding on the origins of hydroxyapatite stabilized gold nanoparticles as high-efficiency catalysts for formaldehyde and benzene oxidation, Catal. Commun. 59 (2015) 195–200, http://dx.doi.org/10.1016/j.catcom.2014.10.028.